

Contents lists available at ScienceDirect

Fuel

journal homepage: www.elsevier.com/locate/fuel





The experimental investigation and data-driven modeling for thermal decomposition kinetics of Green River Shale

Jiahui You, Kyung Jae Lee

Department of Petroleum Engineering, University of Houston, Houston, USA

ARTICLE INFO

Keywords:
Green River Shale
Kerogen thermal decomposition
TGA/DTG
Reaction kinetics
Data—driven modeling

ABSTRACT

Given that kerogen is a source of vast amount of hydrocarbons and organically-bound inorganic elements, it's important to understand the thermal decomposition kinetics of kerogen. Green River Shale contains a significant amount of immature kerogen (Type I), which can be an ideal source for the sample of experimental study. In this study, Thermogravimetric Analysis and Derivative Thermogravimetry (TGA/DTG) was used to quantify the weight loss during the pyrolysis process of the Green River Shale from Utah and subsequently establish the kinetic model of thermal decomposition of kerogen based on the Friedman method followed by the data-driven modeling approach. A two-step reaction mechanism and components of production during the pyrolysis were determined by implementing Thermogravimetry Analysis-Differential Scanning Calorimetry-Gas Chromatography (TGA-DSC-GC). The chemical bonds were analyzed with Fourier-Transform Infrared spectroscopy (FTIR) before and after the pyrolysis. From the experiments, we observed the two-stage reactions in the hydrocarbon evolution window when the heating rate was lower than 30 °C/min, while only one stage was observed with the higher heating rates. C14 hydrocarbon was generated continuously during the hydrocarbon evolution, which indicated that the Green River Shale contained a plentiful amount of it. The kinetic parameters were obtained for the decomposition of organic and inorganic mixture and the organic matter (kerogen) only. The Artificial Neural Network (ANN) method was implemented to train the kinetic parameters obtained from the TGA/DTG experiment. The prediction of extrapolated cases showed a good performance when the heating rate was smaller than 5 °C/min. The generated proxy model can be coupled with various physical models to simulate the thermal decomposition of kerogen with high accuracy.

1. Introduction

Kerogen is a source of vast amount of hydrocarbons and organically–bound inorganic elements, which undergoes thermal cracking and degradation to release them, and it's important to understand the thermal characteristics of kerogen decomposition [1,2]. Green River Shale contains a significant amount of immature kerogen (Type I kerogen), which can provide ideal samples for the thermal experiments. In this study, Thermogravimetric Analysis and Derivative Thermogravimetry (TGA/DTG) was used to quantify the weight loss during the pyrolysis process of the Green River Shale from Utah, to establish the kinetic model of thermal decomposition of kerogen based on the Friedman method and data—driven modeling.

Kerogen thermal decomposition experiments can be conducted using various methods, such as Rock–Eval pyrolysis, pyrolysis–gas chromatography, gold tube pyrolysis, micro–scale sealed vessel pyrolysis, and hydrous pyrolysis [2–6].From the previous studies, we found that

Thermogravimetric Analysis (TGA) is the most appropriate pyrolysis technique for the artificial maturation of the oil shale by the following reasons: TGA method provides non-isothermal temperature programs with wide ranges of heating rates and temperatures; the obtained accurate data of weight loss subjected to temperature can be efficiently used to develop the sophisticated kinetic models; TGA is a widely used technique to heat materials in an inert condition, to figure out their chemical compositions and decomposition reaction kinetics [4]. Numerous studies about TGA on oil shale thermal kinetic models and the characteristics of oil and gas evolution were reported in detail [4-8]. Tiwari provided the TGA-MS data for Green River Shale from Utah with the heating rate from 0.5 °C/min to 10 °C/min and recognized the compounds of molecular weight from 0 to 300 °C [6]. In their work, the uncertainties in activation energies of the thermal kinetic parameters were about 10% for the whole pyrolysis process. Later, the Jimsar oil shale sample was pyrolyzed by TGA under the same heating rate range, and the heating temperature reached 1,000 °C [8]. Kuang identified the

^{*} Corresponding author.

Table 1Results of TOC measurement and Rock–Eval analysis of Green River bulk rock.

Sample I.D. Sample ID	Source quality							Thermal maturity	
	TOC (%)	S1 (mg HC/g rock)	S2 (mg HC/ g rock)	S1 + S2 (mg HC/ g rock)	HI (mg HC / g TOC)	S3 (mg CO2 /g rock)	OI (mg CO2 /g TOC)	Transformation Ratio "PI" (S1/S1 + S2)	T _{max} (°C)
Run 1 Run 2	21.43 20.92	5.63 5.43	185.14 181.27	190.77 186.70	864 866	3.55 3.57	17 17	0.03 0.03	442 443

two–step reaction of the thermal pyrolysis only for the extracted kerogen from Green River Shale [5]. They compared the main isoconversional methods (i.e., Fridman, KAS, and, FWO) and selected the Friedman method with non–linear least–squares analysis to establish the kinetic models of two–step reaction. The heating rates for the pyrolysis ranged from 2 °C/min to 20 °C/min to figure out the kinetic parameters. Numerous studies established the pyrolysis kinetic models using the traditional isoconversional methods, which are only effective under the specific heating rate range and the extension of conversion.

Recently, several investigations have applied the machine learning methods in studying the thermal reaction kinetics with high accuracy and flexibility [9–11]. Artificial Neural Network (ANN) method was employed to predict the organic matter contents and activation energy in the investigation of the in–situ pyrolysis of kerogen [9]. A recent study used the ANN approach to validate the results from the distributed activation energy model of Staghorn Sumac decomposition [10]. Hosen et al. combined the ANN method and conventional model to predict the kinetic parameters for the polymerization batch reaction. The obtained hybrid model showed higher accuracy than the other previously published kinetic models [11].

Previous study found that only the Green River Shale generated a relatively large amount of prist-1-ene and isoalkanes during the stepwise pyrolysis, which denoted that the organic matters from Green River Shale was different from other types of shales [4]. In addition, the Utah Geologic Survey indicated that the lacustrine source rocks with Type I kerogen in the Brazilian Campos and Santos basins alone were responsible for more than 5.5 billion barrels of oil production between 2004 and 2013. However, only 0.7 billion barrels have been produced from Green River Shale of Uinta Basin [12,13]. Thus, the Green River Shale of Uinta Basin still has a vast potential of hydrocarbon resources to be exploited. To the best of our knowledge, there's no study on the data--driven modeling of thermal decomposition kinetic models of shale rock and kerogen by applying the ANN approach, which is significantly effective to build proxy models for the datasets with nonlinearity. In addition, no data-driven model has been established using the experimental data of Green River Shale. In this regard, our study on the thermal decomposition kinetics focuses on the Green River Shale from Uinta Basin to elucidate the kerogen decomposition mechanisms and establish the data-driven models.

In this work, we aim to investigate the evolution of generated hydrocarbons during the kerogen thermal decomposition and establish the reaction kinetics of Green River Shale from Utah. We obtained the weight loss of the bulk rock and the pyrolysis of isolated kerogen using TGA/DTG. Then, the two-step reaction mechanisms and components of production of the kerogen thermal decomposition were determined by implementing TGA-DSC-GC. The FTIR analyzed the chemical bonds before and after the pyrolysis. The thermal kinetic parameters were established by the Friedman method, and the probable kinetic model was evaluated by the Popescu method. The Artificial Neural Network (ANN) method was firstly implemented to train the dataset involving the information of kinetic parameters and heat flow of the Green River Shale. By applying the ANN method, the generated data-driven model can predict the kinetic parameters within the training range with high accuracy and efficiency, given that the experimental method is not only expensive but also time-consuming. Once the ANN model has been trained, the output can be obtained in a second. The generated

data–driven model can also be coupled with various numerical models to simulate the thermal decomposition of kerogen with high accuracy. This paper is organized as follows: the experimental and theoretical methods are addressed in Section 2; Section 3 analyzes the experimental results and presents the developed kinetics models; the summary and conclusion are included in Section 4.

2. Experimental and theoretical methods

2.1. Samples preparation

In this experiment, we considered both the bulk rock shale and the isolated kerogen from the Green River formation. To decrease the impacts of the mineral heterogeneity on the reaction kinetics modeling of organic matter, the bulk rock shale was ground and sieved as smaller than 0.25 mm-diameter before pyrolysis. The kerogen isolation was conducted in the closed-conservative ultra-pure kerogen isolation at the Center for Petroleum Geochemistry at the University of Houston. The closed-conservative kerogen isolation method is very effective in removing the impure fractions [14]. The bulk rock of Green River Shale specimens was put into Teflon cells and flushed by HCl several times to dissolve carbonate, sulfates, and soluble sulfides. Then, the specimens were flushed by HF to dissolve siliciclastic, ammonium hydroxide to neutralize the system and remove HCl soluble gels [14]. During each step of flush, the specimens were rinsed with deionized water. Finally, the specimens were put into acidic CrCl2 to dissolve pyrite in the sealed reaction cells.

2.2. Thermogravimetric analysis

The TGA/DTG analysis was carried out using the Perkin Elmer STA 6000. Approximately 20 mg of the sample for the bulk rock and isolated kerogen were put in the pan kit. The samples were heated from 30 to 990 $^{\circ}\text{C}$ with the heating rates from 1 $^{\circ}\text{C/min}$ to 100 $^{\circ}\text{C/min}$ under a constant helium flow rate of 20 ml/min.

2.3. TGA-DSC-GC and FTIR

A hyphenated system of TGA-DSC-GC was used to simultaneously analyze the gas components while heating samples at the heating rate of 5 °C/min, 20 °C/min, and 50 °C/min. TGA was used to measure the weight change of the sample, and Differential Scanning Calorimetry (DSC) was used to measure the heat flow of the sample. Gas components were analyzed by the GC of Perkin Elmer Clarus 590. The outlet of the TGA heating chamber was connected to Clarus 590 by TG-GCMS Interface TL 8500. Elite-VMS column with 40 m length, 0.18 mm ID was used to separate the compositions. First, the isothermal temperature program for the GC oven was set at 40 °C and held for 30 min. Then, the oven temperature was increased to 260 °C with the rate of 5 °C/min and hold for 3 min. The injector temperature was set at 250 $^{\circ}$ C; split vent flow was set as 100 ml/min; and the carrier gas flow rate was 0.7 ml/ min. We collected the volatile gas for 0.5 min at each reaction stage of the pyrolysis. The target gas components were alkanes and aromatics. We directly injected two standards sample—D2887 and DHA aromatics into GC to establish the GC library to interpret the peaks of GC results [15,16]. Fourier Transform Infrared Spectroscopy (FTIR) was used to

Table 2 Kinetic models $(f(\alpha))$ and their integral expressions $(g(\alpha))$.

Model	f(a)	$g(\alpha)$
Reaction–order model		
First–order (F1)	$(1-\alpha)^1$	$-\ln(1-lpha)$
Second-order (F2)	$(1-\alpha)^2$	$\left(1-lpha ight)^{-1}-1$
Third-order (F3)	$(1-\alpha)^3$	$\left[(1-lpha)^{-2}-1\right]/2$
Nucleation model		L J/
Power law (P2)	$2lpha^{1/2}$	$lpha^{1/2}$
Power law (P3)	$3lpha^{2/3}$	$lpha^{1/3}$
Power law (P4)	$4a^{3/4}$	$lpha^{1/4}$
Avrami–Erofe've (A2)	$2(1-\alpha)[-\ln(1-\alpha)]^{1/2}$	$\left[-\ln(1-\alpha)\right]^{1/2}$
Avrami–Erofe've (A3)	$3(1-\alpha)[-\ln(1-\alpha)]^{2/3}$	$\left[-\ln(1-\alpha)\right]^{1/3}$
Avrami–Erofe've (A4)	$4(1-\alpha)[-\ln(1-\alpha)]^{3/4}$	$\left[-\ln(1-\alpha)\right]^{1/4}$
Geometrical contraction model		
Contracting area (R2)	$2(1-\alpha)^{1/2}$	$1 - (1 - a)^{1/2}$
Contracting volume (R3)	$3(1-lpha)^{2/3}$	$1 - (1 - \alpha)^{1/3}$
Diffusion model		
1–D diffusion (D1)	$1/2\alpha$	α^2
2–D diffusion (D2)	$-1/\ln(1-lpha)$	$-[(1-lpha){ m ln}(1-lpha)]+lpha$
3–D diffusion (D3)	$3(1-\alpha)^{2/3}/\Big[2\Big(1-(1-\alpha)^{1/3}\;\Big)\;\Big]$	$- \Big\lceil 1 - (1-\alpha)^{1/3} \Big\rceil^2$
Ginstling-Brounshtein (D4)	$3/2\Big[(1-\alpha)^{-1/3}-1\Big]$	$1 - (2\alpha/3) - (1 - \alpha)^{2/3}$

scan the sample and observe chemical properties by the infrared light. The chemical bonds were measured before and after heating the sample.

2.4. Rock-Eval analysis

Rock–Eval Analysis was conducted by Vinci RockEval–6 Pyrolysis Analyzer on the bulk rock of Green River Shale. The detailed results for Rock–Eval analysis are listed in Table 1. The Total Organic Carbon (TOC) was found to be about 21 wt% from the twice replicate measurements. S1 is the free hydrocarbons present in the sample before the analysis; S2 is the volume of hydrocarbons formed during the thermal pyrolysis; S3 is the amount of $\rm CO_2$ produced during the pyrolysis of kerogen [17]. The HI and OI are Hydrogen Enrichment Index and Oxygen Enrichment Index, which indicate that the bulk rock of Green River Shale contained Type I kerogen. $T_{\rm max}$ values for the bulk rock samples were 442 and 443 °C, indicating that the Green River Shale kerogen has from low to marginal thermal maturity [18].

2.5. Theoretical methods for reaction kinetics

The rate equation of non-isothermal pyrolysis kinetics can be expressed as the following equation [19]:

$$kf(\alpha) = \frac{d\alpha}{dt} = \beta \frac{d\alpha}{dT} = Aexp(-\frac{E_a}{RT})f(\alpha)$$
 (1)

where, α is the degree of conversion; β is the heating rate (°C/min); k is the reaction constant; E_a is the activation energy (J/mol); A is the pre–exponential factors (min⁻¹); R is the universal gas constant, which equals to 8.314 J/K·mol, and T is the temperature (K). α can be calculated by the following equation:

$$\alpha = \frac{W_O - W_t}{W_0 - W_m} \tag{2}$$

where, W_O is the initial mass of the sample; W_t is the mass at time t, and W_∞ is the final mass after the pyrolysis. We selected the linear Friedman method to estimate E_a in the rate equation, since it directly used the differential form of the rate equation and did not require any mathematical approximations, which could avoid calculation errors [5].

Application of the logarithm of the Eq.1 provides the following equation by Friedman method:

$$\ln\left(\beta \frac{d\alpha}{dT}\right) = \ln\left(\frac{d\alpha}{dt}\right) = \ln[Af(\alpha)] - \frac{E_a}{RT}$$
(3)

where, $\frac{d\alpha}{dt}$ was obtained numerically from the TGA experiments data with $\Delta\alpha=0.02$. First, we plotted the graph taking $\ln\left(\frac{d\alpha}{dt}\right)$ as y-axis and $\frac{1}{T}$ as x-axis under the constant α for a set of β values. Then we found the slope of $-\frac{E_{\alpha}}{R}$ with the series of straight line [19]. To find the most suitable kinetic model, we used the Popescu method, while taking advantages of no assumptions and insensitivity of potential experimental errors [5].

By taking the integral expression of Eq. (3), we obtain the following equation:

$$\int_{\alpha_m}^{\alpha_n} \frac{d\alpha}{f(\alpha)} = \frac{1}{\beta} \int_{T_m}^{T_n} k(T) dT \tag{4}$$

where a_n and a_m are corresponding degree of conversion at temperature of T_n and T_m . By using the notations:

$$g(\alpha) = \int_{a_m}^{a_n} \frac{d\alpha}{f(\alpha)}$$
 (5)

and.

$$I(T)_{nm} = \int_{T}^{T_n} k(T)dT \tag{6}$$

Eq. (4) can be substituted into the following form:

$$g(\alpha) = \frac{1}{\beta}I(T)_{nm} \tag{7}$$

For each pair of the temperature range (ie., T_n and T_m), we can find corresponding degree of conversion (ie., $(\alpha_{n1}, \alpha_{m1}), (\alpha_{n2}, \alpha_{m2}), (\alpha_{n3}, \alpha_3)$...) under the different heating rates of β (ie., β_1 , β_2 , β_2 ...) from the experimental data [5]. The possible kinetic models ($f(\alpha)$) and their integral expressions ($g(\alpha)$) are listed in Table 2. Then, the integral expression value of each kinetics model (ie., $g(\alpha)_{nm1}, g(\alpha)_{nm2}, g(\alpha)_{nm3}$...) can be calculated. We plotted the linear fitting curve of $g(\alpha)$ and $\frac{1}{\beta}$ with y-intersect of zero and calculated coefficient of determination (R^2) for the fitting curve of different kinetic models. For different pyrolysis stages, a proper kinetic model can be selected by considering R^2 value.

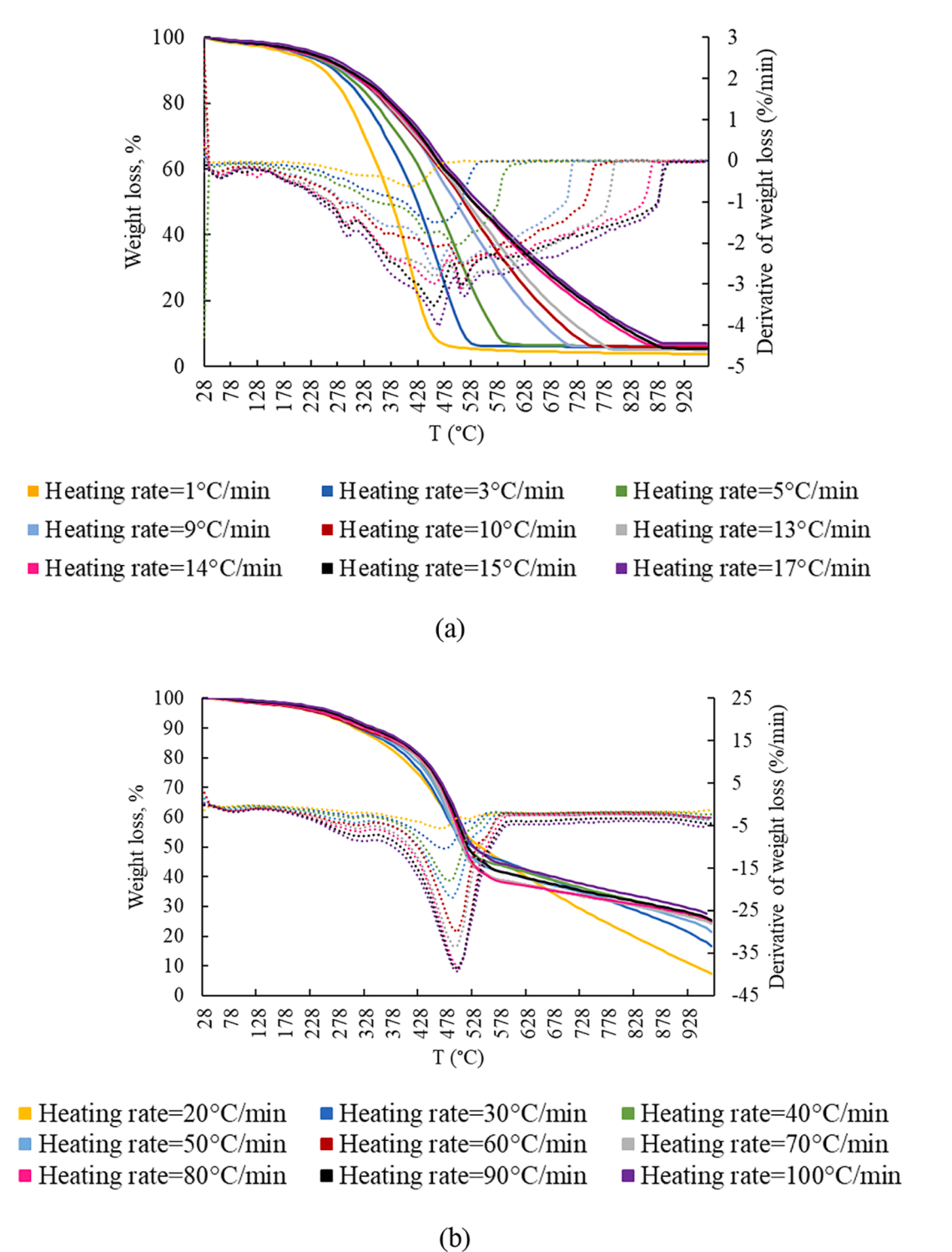


Fig. 1. The normalized weight loss curve and derivative under the heating rates from (a) 1 °C/min to 17 °C/min and (b) 20 °C/min to 100 °C/min of isolated kerogen. The solid line denotes the normalized weight loss, and the dot line denotes the derivative of weight loss.

2.6. ANN method

The ANN multi-layer model contains the input, hidden, and output layers [20]. We selected different neuron numbers for training data sets under different temperature ranges to achieve high performance. The neurons process the combined information of inputs, weights, biases, activation functions to produce the outputs [21]. Bias assures the diversity of the model formats and guarantees the best performance of training [21]. In this study, hyperbolic tangent (tanh) activation

function was used to restrict the output within the required range. He–uniform variance scaling initializer was used to initialize the weight value following the uniform distribution within [-limit, limit], where limit was depending on the number of input units [22]. We selected the Mean Squared Error (MSE) loss function to evaluate the difference between the training data and the predicted value. The Back–propagation algorithm was used to train the neural network model. ADAM algorithm optimizer was employed to decrease the loss function to the convergence criteria by iteratively calculating the gradient of the loss function and

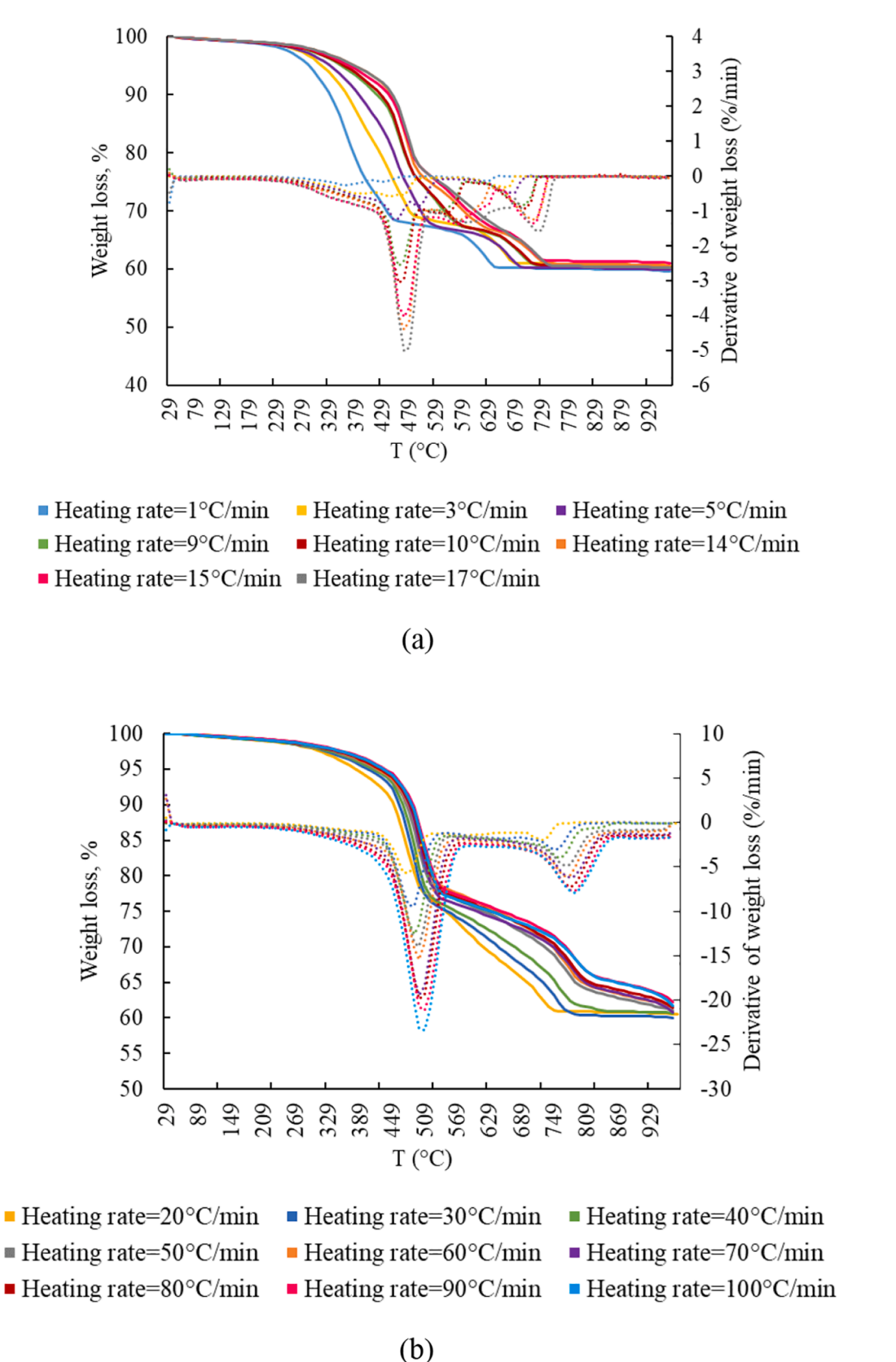


Fig. 2. The normalized weight loss curve and derivative under the heating rates from (a) 1 $^{\circ}$ C/min to 17 $^{\circ}$ C/min and (b) 20 $^{\circ}$ C/min to 100 $^{\circ}$ C/min of bulk rock shale. The solid line denotes the normalized weight loss, and the dot line denotes the derivative of weight loss.

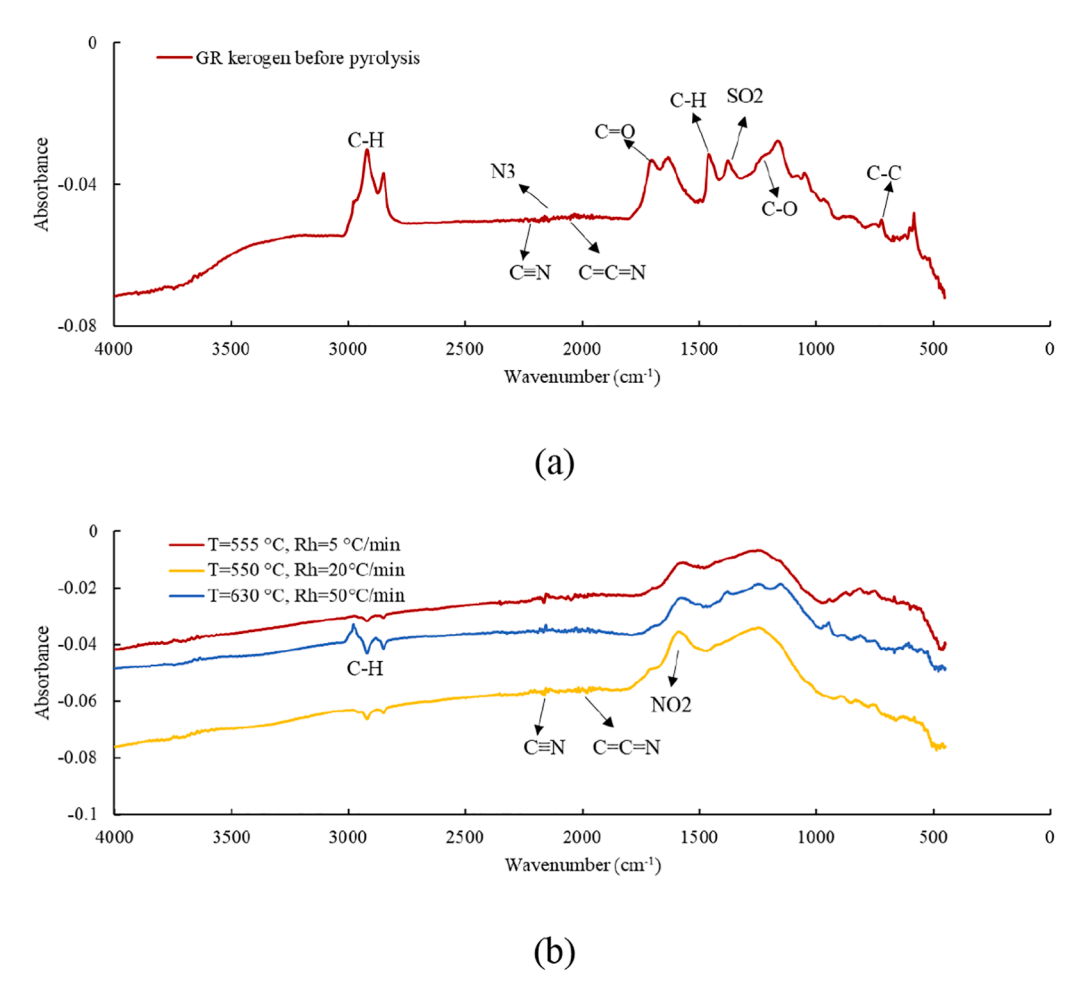


Fig. 3. FTIR results for Green River kerogen. (a) FTIR results before pyrolysis; (b) FTIR results within the hydrocarbon window (200–620 °C). (For interpretation of the references to colour in this figure legend, the reader is referred to the web version of this article.)

updating the weight and bias [23]. The training rate was set as 0.001, and the convergence criteria was set as 1×10^{-5} . The ANN method was developed based on TensorFlow open–source software library [24].

3. Results and discussion

The present study investigates the thermal characteristics during TGA/DTG pyrolysis of isolated kerogen and bulk rock of Green River Shale. The TGA/DTG results and the produced components are described in Sections 3.1 and 3.2. The kinetic models were established using the Freidman method and Popescu method by using the experimental results. The ANN-based data-driven modeling method was employed to predict the parameters of reaction kinetics by taking the heat flow as an input, which is introduced in Section 3.4.

3.1. Thermogravimetric analysis of samples

This work measured weight loss of samples during the thermal decomposition of bulk rock shale and isolated kerogen with the heating rates from 1 $^{\circ}$ C/min to 100 $^{\circ}$ C/min. The heating temperature profile was set at 30–990 $^{\circ}$ C. The previous study shows that the main components of Green River Shale rock from Utah were quartz, albite, calcite, illite, dolomite, orthoclase, aragonite, and analcime [6]. The change of weight loss with time and its derivative are shown in Fig. 1 and Fig. 2. From the derivative of weight loss, we could observe a two–step decomposition reactions for bulk rock shale and a single–step reaction for isolated kerogen. For the Green River bulk rock, the first reaction was around 320–620 $^{\circ}$ C, and the second reaction was around 650–850 $^{\circ}$ C. For the

lower temperature region of up to 200 °C, the evaporation of moisture, interplay water, clay minerals, and nahcolite (carbonate) minerals resulted in the weight loss [25]. The decomposition window of the nahcolite was between 50 °C and 200 °C [26]. The mineral decomposition rate was also influenced by the heating rate. When the heating rate was high, the decomposition rate of mineral was low, and the weight loss was small. Since we used dry samples of kerogen and bulk rock shale, there was no obvious weight loss during this temperature window. The volatile hydrocarbon is known to be generated from shales during the temperature window of 200–620 °C and results in weight loss during thermal decomposition [25].

For the two-step reaction of bulk rock shale, the weight loss for temperature beyond 600 °C was due to the carbonate decomposition [25]. The carbonate was removed from the kerogen, and there was only a single-step reaction for isolated kerogen. For the pyrolysis of isolated kerogen, we could observe the two-step evolution of hydrocarbons within 200 °C to 620 °C of temperature at the heating rates from 5 °C/ min to 30 °C/min, as shown in Fig. 1 (a) and (b). The previous pyrolysis studies showed that Kimmeridge oil shale, Jordanian oil shale, Turkish oil shale, and Green River Shale had two-step decomposition for hydrocarbons [25,27-29]. However, the two-step evolution for hydrocarbons was not obvious with the heating rates higher than 30 °C/min. It could be caused by that the different components from the sample were not detected due to the fast increase of temperature. The weight loss percentage is listed in the SI. Under the lower heating rates, the sample showed larger weight loss at the end of the pyrolysis. Given that the sample was heated for a long time under the lower heating rate, the weight loss was found to be highly influenced by the heating time.

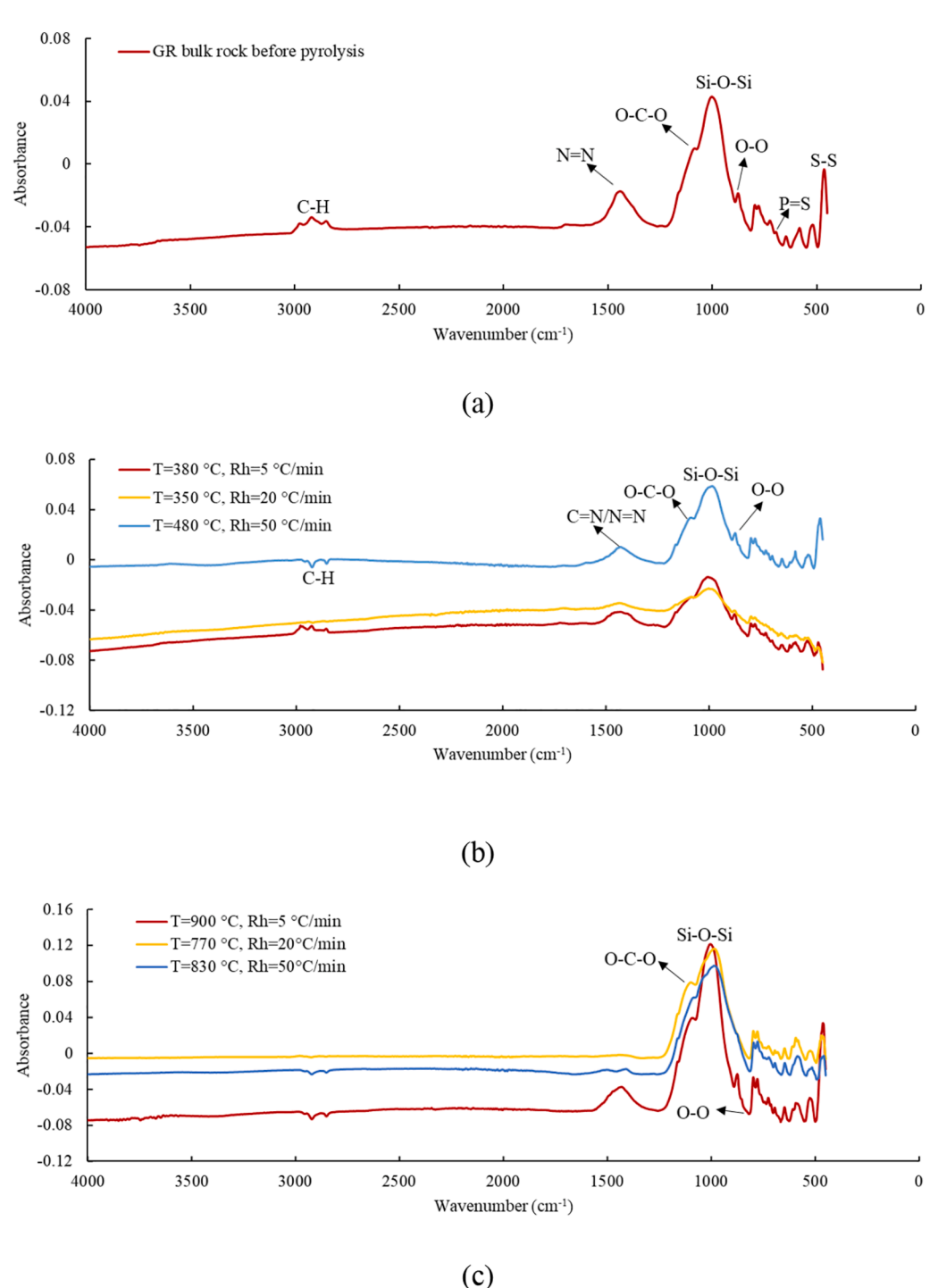


Fig. 4. FTIR results for the bulk rock of Green River Shale. (a) FTIR results before pyrolysis; (b) FTIR results within the hydrocarbon window (200–620 $^{\circ}$ C); (c) FTIR results after the second step reaction (temperature larger than 620 $^{\circ}$ C). (For interpretation of the references to colour in this figure legend, the reader is referred to the web version of this article.)

3.2. TGA-DSC-GC and FTIR results

We conducted the FTIR analysis on the isolated kerogen and bulk rock of Green River Shale before and after the pyrolysis. We selected some temperature to conduct FTIR analysis during the hydrocarbon decomposition stage. Then we performed additional analyses after the second step reaction (temperature higher than 620 $^{\circ}\text{C}$) for the bulk rock shale. The chemical bonds representing certain peaks and corresponding wavelengths are listed in SI. Fig. 3 shows the FTIR results before and after the pyrolysis of isolated kerogen. The bonds between 2,864–2,843

cm $^{-1}$ and 2,936–2,916 cm $^{-1}$ indicate stretching C–H. The symmetrical stretching C–H bond from 3,000 to 2,900 cm $^{-1}$ can be indicating the cyclohexyl group. The compound containing C–H is mainly aliphatic hydrocarbons and aromatic hydrocarbons [7]. Vibration of C–H bonds in the range of 720 cm $^{-1}$ to 750 cm $^{-1}$ are the aromatic rings and unsaturated aliphatic hydrocarbon. Stretching C=N and C=C=N bonds between the wavelength of 2,210–2,175 cm $^{-1}$ and 2,050–2,000 cm $^{-1}$ are in the nitrogen compounds [30]. The mean nitrogen content in oil shale is about 1.3% [31]. Stretching bond C=O from 1,186 cm $^{-1}$ to 1,168 cm $^{-1}$ and N $_3$ from 2,155 cm $^{-1}$ to 2,141 cm $^{-1}$ are in the functional

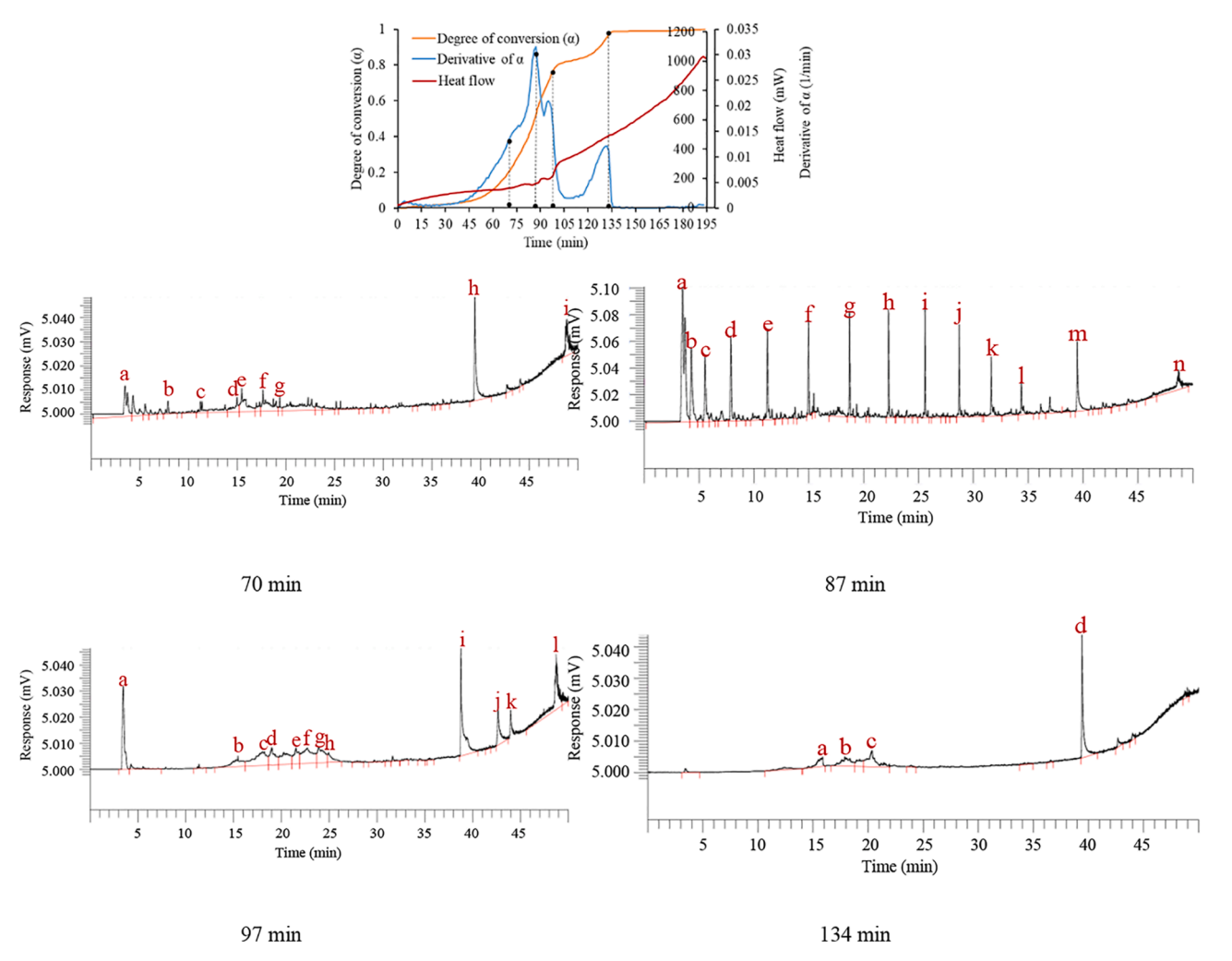


Fig. 5. The results of TGA/DTG and heat flow and the results of GC analysis for bulk rock shale pyrolysis under the heating rate of 5 °C/min. GC components were analyzed at t = 70 min, 87 min, 97 min, and 134 min.

Table 3GC components produced at different times for the bulk rock pyrolysis at 5 °C/min–heating rate.

Peak	Retention time (min)	Area %	Component formula	Peak	Retention time (min)	Area %	Component formula
70 min				87 min			
a	3.46	14.39	*	a	3.487	22.49	*
b	7.88	1.81	*	b	4.278	6.48	*
c	11.22	2.57	C5H10/C5H8	c	5.532	4.85	*
d	14.96	4.23	C6H10	d	7.888	5.01	*
e	15.46	8.31	C7	e	11.227	5.45	C5H10/C5H8
f	17.64	9.11	C7H12	f	14.985	3.67	C6H10
g	20.45	11.44	C8H12	g	18.719	3.96	C7H10
h	39.41	13.67	C14	h	22.267	3.81	C8H12
i	48.92	8.62	*	i	25.596	3.46	C10
97 min				j	28.711	4.4	C11
a	3.458	10.26	*	k	31.625	3.39	C11H22/C11H20/C12H18
b	15.455	4.78	C7	1	34.369	2.32	*
c	18.028	10.51	C7H12	m	39.467	4.6	C14
d	18.995	5.78	C8	n	48.704	5.54	*
e	21.519	4.4	C8H12	134 min			
f	22.667	10.16	C9H18	a	15.871	8.77	C7H14
g	23.91	6.34	C9H12	b	17.903	14.03	C7H12
h	24.932	2.63	C10H14	c	20.359	21.04	C8H12
i	38.764	13.74	C13H*	d	39.42	30.96	C14
j	42.656	5.51	*				
k	48.723	13.12	*				
1	49.465	1.57	*				

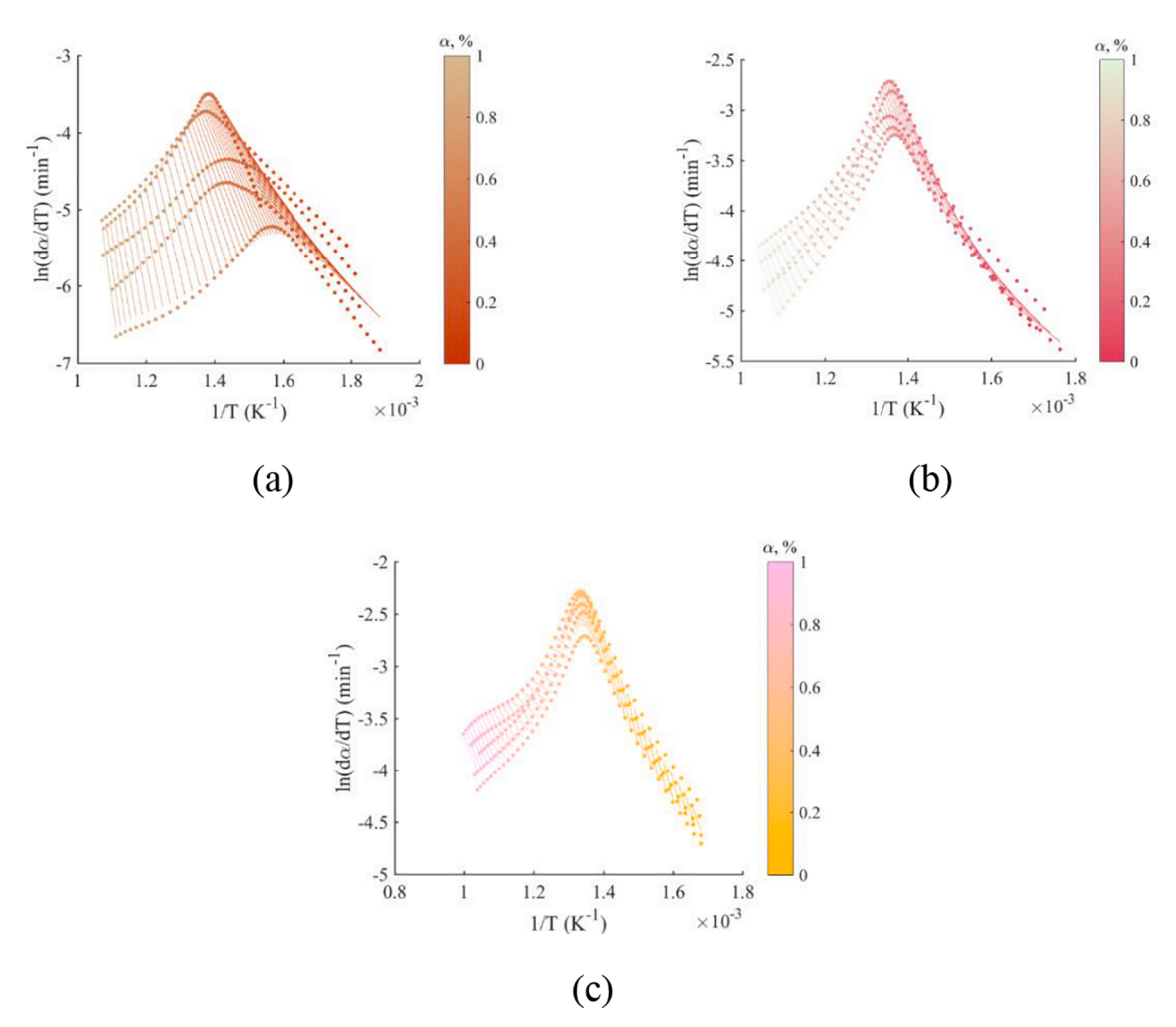


Fig. 6. The plots for $\ln\left(\frac{d\alpha}{dt}\right)$ and 1/T according to Friedman method of non–isothermal bulk rock shale pyrolysis. The slope represents the value of $-\frac{E_a}{R}$, and then we can obtain the activation energy. (a) heating rates from 1 °C/min to 5 °C/min; (b) heating rates from 6 °C/min to 10 °C/min; (b) heating rates from 10 °C/min to 20 °C/min.

group of C-(C=O)–N₃. The peak at 1,360–1,390 cm⁻¹ is the SO₂ bond. For the peak between 1,300–1,160, the possible chemical bond is C-O, which is in the functional group of C=C-COOR. Before the reaction, the sample contain the functional group of R(CH₂)₄-C/R(CH₂)₄-OR, Cyclohexyl, C=C-COOR, C-(C=O)–N₃, and Si-O-Si- $_6$ member ring. After the pyrolysis of isolated kerogen, as shown in Fig. 3 (b), the detected chemical bonds are C–H, C \equiv N, C=C=N, and NO₂ within the hydrocarbon decomposition temperature window [30]. During pyrolysis, the chemical bond of C–H was broken. The degree of C–H bond broken depended on the heating rate and heating time. When the heating rate was 50 °C/min, it took a shorter time to reach 630 °C and left some C–H bonds unbroken. Thus, the peak of C–H bond was obvious at 630 °C with hating rate of 50 °C/min. At this time, the functional group (R)₂C=N-C \equiv N, (C)₂C=C=N-R, Cyclohexyl, R(CH₂)₄-C/R(CH₂)₄-OR still remain in the sample. There is a new functional group N-NO₂ after the pyrolysis.

Fig. 4 shows the FTIR results for the pyrolysis of bulk rock shale. Before pyrolysis, we detected Si-O-Si, P=S, S-S bonds, which were not found from kerogen sample. Si-O-Si probably existed in the Si-O-Si $_6$ -member ring functional group, and this chemical bond was not easy to crack during the pyrolysis. Si-O-Si might have come from the quartz in shale bulk rock. Other possible functional groups have C-N=NH-C, R-S-S-R, R-O-O-R, R(CH₂)₄-C/R(CH₂)₄-OR and Cyclohexyl. The peaks during 800–580 cm⁻¹ can be assigned to P=S, which can be contained in minerals in the bulk rock shale. Stretching S-S bond was in the range of 450–480 cm⁻¹, which denoted a disulfide compound in the bulk rock

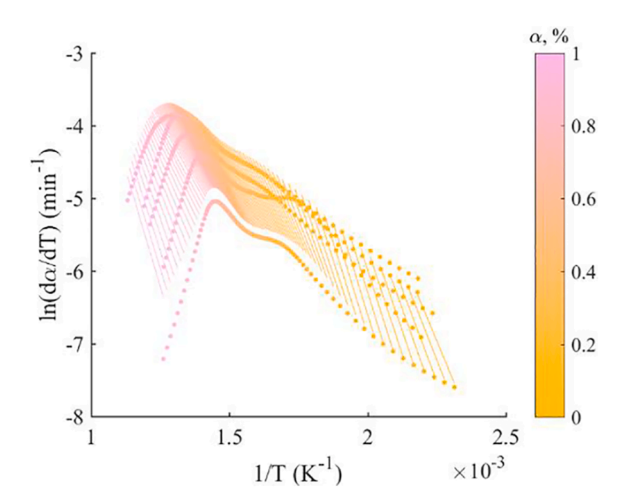


Fig. 7. The plot for Friedman method of non–isothermal pyrolysis of isolated kerogen with heating rate from 1 $^{\circ}$ C/min to 5 $^{\circ}$ C/min.

shale. After the pyrolysis of bulk rock shale, the C–H bond cracked and became weak. $Si-O-Si_6$ -member ring functional group still exists in the sample.

GC analysis was conducted simultaneously during the pyrolysis. We

Table 4 R^2 for different kinetic models of bulk rock pyrolysis.

model	Temperature range(°C)								
	150–300	300–350	350–400	400–450	450–650	650–700			
First–order (F1)	_	0.81	0.91	_	_	0.88			
Second-order (F2)	0.072	0.91	0.98	0.93	0.94	0.56			
Third-order (F3)	0.23	0.96	0.94	0.98	0.86	0.37			
Power law (P2)	_	_	_	_	_	_			
Power law (P3)	_	_	_	_	_	_			
Power law (P4)	_	_	_	_	_	_			
Avrami-Erofe've (A2)	_	_	_	_	_	0.93			
Avrami-Erofe've (A3)	_	_	_	_	_	0.94			
Avrami-Erofe've (A4)	_	_	_	_	_	0.94			
Contracting area (R2)	_	0.73	0.76	_	_	0.89			
Contracting volume(R3)	_	0.75	0.83	_	_	0.94			
1–D diffusion (D1)	_	_	_	_	_	_			
2-D diffusion (D2)	0.94	0.97	0.97	0.59	_	0.80			
3-D diffusion (D3)	0.95	0.96	0.96	0.85	_	0.91			
Ginstling-Brounshtein (D4)	0.94	0.97	0.97	0.70	_	0.93			

Table 5 R² for different kinetic models of pyrolysis of isolated kerogen.

model	Temperature range(°C)								
	150–300	300–350	350–400	400–450	450–500				
First–order (F1)	_	0.37	0.99	0.99	0.80				
Second-order (F2)	_	0.74	0.84	0.84	0.57				
Third-order (F3)	_	0.91	0.71	0.71	0.44				
Power law (P2)	_	_	_	_	_				
Power law (P3)	_	_	_	_	_				
Power law (P4)	_	_	_	_	_				
Avrami-Erofe've (A2)	_	_	0.83	0.83	0.91				
Avrami-Erofe've (A3)	_	_	0.60	0.60	0.93				
Avrami-Erofe've (A4)	_	_	0.38	0.38	0.93				
Contracting area (R2)	_	_	0.74	0.74	0.91				
Contracting volume(R3)	-	0.17	0.90	0.90	0.89				
1–D diffusion (D1)	_	_	_	_	_				
2-D diffusion (D2)	0.78	0.93	0.94	0.94	0.84				
3-D diffusion (D3)	0.82	0.96	0.95	0.95	0.73				
Ginstling-Brounshtein (D4)	0.79	0.94	0.97	0.97	0.80				

collected the decomposed gas from TGA pyrolysis for 0.5 min. Fig. 5 shows the results for the GC analysis under the heating rate of 5 $^{\circ}$ C/min. The results for 20 $^{\circ}\text{C/min}$ and 50 $^{\circ}\text{C/min}$ can be found from SI. The degree of conversion (α), derivation of α , and heat flow were plotted in Fig. 5. We can observe three peaks on the curve of the derivative of α , along with endothermic characteristics on the heat flow curve. For heating rate of 5 °C/min, the two endothermic characteristics occurred at around t = 87 min and t = 97 min, respectively, when the shale was decomposed into hydrocarbons. Gas was collected at these three derivative peaks for GC components analysis. The gas components are listed in Table 3. The star symbol (*) in the table denotes that the component was out of our column range, which could not be identified. The pyrolysis of bulk rock shale produced the maximum number of components at t = 87 min when the heating rate was 5 °C/min, which was also the maximum peak of the derivative of α . We named the peak of derivative of α as the maximum derivative for clarity. The pyrolysis of the bulk rock shale mainly produced alkenes, alkanes, and aromatics. We could get very limited amount of hydrocarbons at t = 70 min (at 380 °C). C10, C11 and C14 were the main alkane components produced at t = 87 min, whereas C7 and C8 were the main alkane components at t= 97 min. At t = 134 min, C14 was the only alkane produced at this time. For the larger heating rates, the second-step reaction showed a shorter time, and there was no clear boundary for the generation of different components. Other components occurred only at the maximum derivative. GC results for isolated kerogen showed similar results, which are provided in the SI.

3.3. Thermal kinetic models

weight loss for the isolated kerogen is only account for the pure kerogen decomposition. Thus, the kinetic parameters obtained from heating the bulk rock were valid for the mixture of organic matter and minerals, while the ones from heating the kerogen samples were valid for the pure organic matter. Each plot takes five sets of $\ln\left(\frac{da}{dt}\right)$ and the corresponding temperature under different heating rates. Fig. 6 (a) and Fig. 7 are for the heating rates from 1 °C/min to 5 °C/min, and Fig. 6 (b) is for the heating rates from 6 °C/min to 10 °C/min. The plots in Fig. 6 (c) have the heating rates of 12 °C/min, 14 °C/min, 16 °C/min, 17 °C/min, and 20 °C/min. The plots for different degrees of conversion with $\Delta\alpha=0.02$ are shown in different colors. R^2 for the prediction of $\Delta \alpha$ by the thermal kinetic model of Friedman could reach 0.991. We built the kinetic model of kerogen decomposition with the heating rates from 1 °C/min to 5 °C/ min, since the pyrolysis of isolated kerogen was highly sensitive to the heating rates, and the higher heating rate could lead to significant error on the kinetic model by using both Friedman method and data-driven method. The obtained activation energy and the value of y-intersect are listed in the SI.

The isoconversional plots of the Friedman method for bulk rock shale

and kerogen are shown in Fig. 6 and Fig. 7, respectively. The weight loss

for the bulk rock of Green River accounts for the evaporation of moisture, interplay water, clay minerals, nahcolite, and kerogen. While the

The most probable kinetic model was determined by the Popescu method [5]. For different reaction stages, the decomposition has

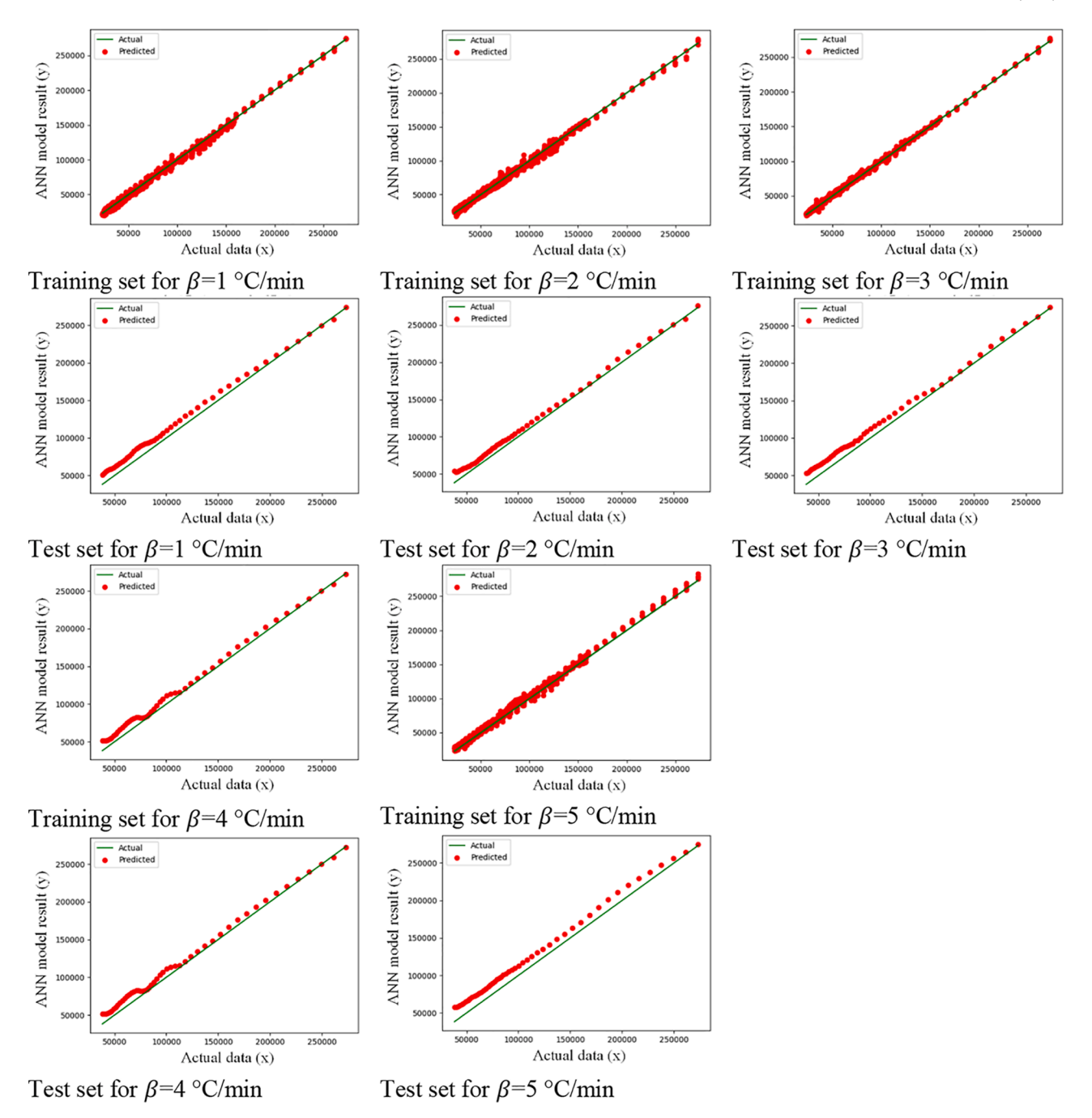


Fig. 8. Performance of the data-driven models of bulk rock shale on activation energy (J/mol).

different kinetic parameters and needs an appropriate kinetics model. We divided the pyrolysis process into six stages for bulk rock shale and five stages for kerogen, respectively. R^2 of the possible kinetic model was calculated for each stage by temperature. The expression of the kinetic models is listed in Table 2. The corresponding degree of conversion under different temperatures is listed in the SI. Some values are not indicated in the table for kinetic models, because their functions couldn't be established based on the described method. The diffusion models are generally suitable for the temperature range of 450–650 °C. Between 450 and 650 °C, the second–order reaction model was the most probable model for bulk rock shale, since it has the highest R^2 value according to Table 4, and Avrami–Erofe've Nucleation models were more suitable for the pyrolysis of isolated kerogen (Table 5).

3.4. ANN results

We performed ANN training on the dataset of the kinetic parameters, where the input data included Δa , heat flow, and heating rate, and the output data included the activation energy and $\ln[Af(\alpha)]$. The raw data for ANN training is provided in the SI. We first randomly selected 20% data as the test set, and the other 80 % data was used as the training set. We have 750 datasets for the bulk rock shale and 250 in total for the isolated kerogen. The performance of bulk rock parameters and kerogen were shown in SI.

To see the performance of predicting the data out of our training set, we picked the data under one designated heating rate as the test set and the remaining data sets as the training set, instead of a random manner. Thus, the training sets didn't contain the data under the same heating rate as the test sets. For the bulk rock shale, training data has 700 sets,

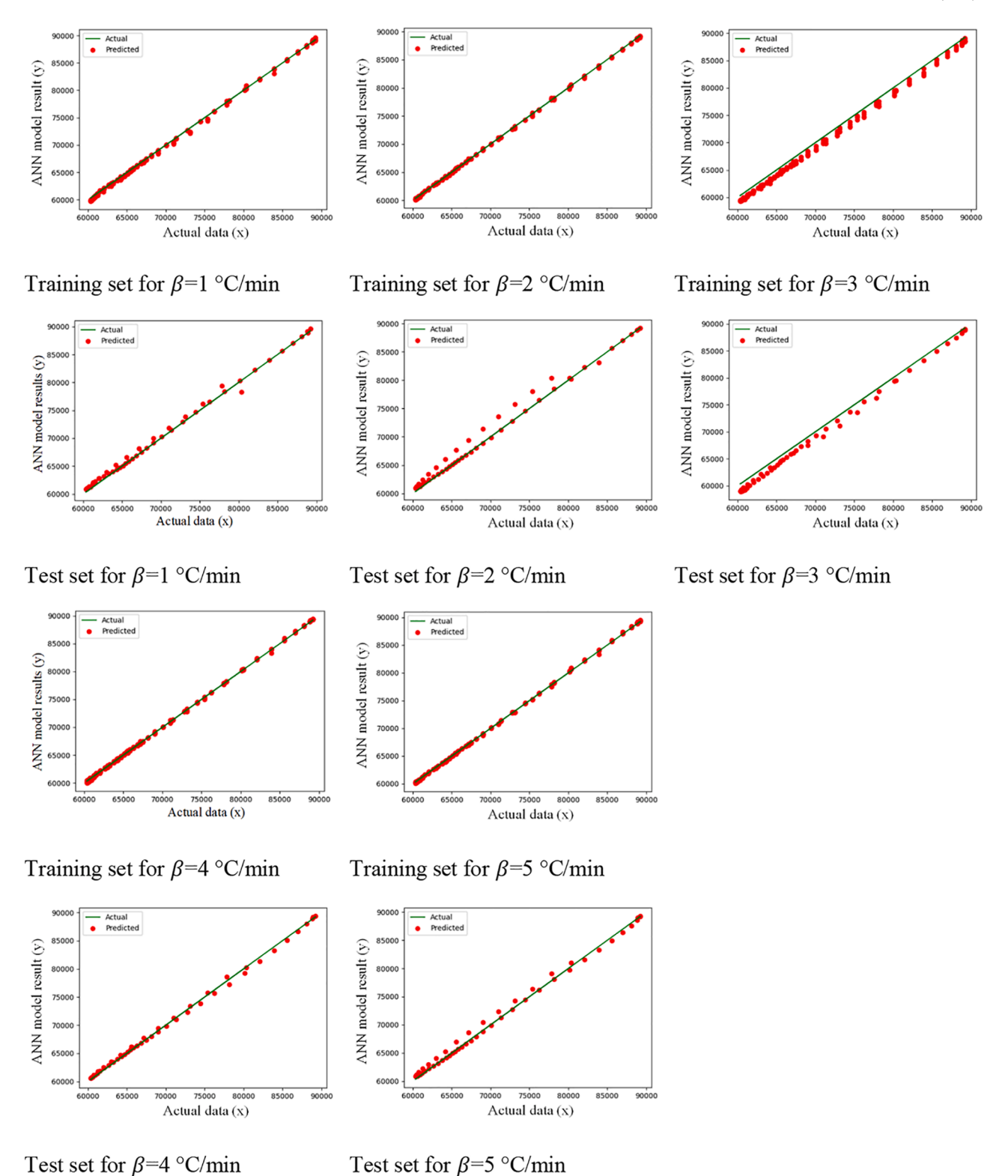


Fig. 9. Performance of the data-driven models of kerogen on activation energy (J/mol).

and test data has 50 sets. We found that the performance was good for the heating rate from 1 °C/min to 5 °C/min of both isolated kerogen and bulk rock shale. As shown in Fig. 8, R2 for predicting bulk rock shale's activation energy could reach 0.997. For the test set, R² was 0.973, 0.984, 0.971, 0.984, and 0.954 for heating rates for 1, 2, 3, 4, and 5 °C/min. We got similar R² for predicting $ln[Af(\alpha)]$ between 1 °C/min and 5 °C/min. However, 80 neurons were used to reach high R² for training

 $ln[Af(\alpha)]$. The performance plot and scattered distribution for $ln[Af(\alpha)]$ were shown in the SI. Fig. 9 shows the performance of the ANN model for kinetic parameters of kerogen decomposition. We used 200 datasets for training and 50 datasets for the test. Thus, the neuron number was increased to 100 to get the high R^2 . The ANN training took 5,000 steps to meet the convergence criteria. R^2 could reach 0.999 for the prediction of activation energy and $ln[Af(\alpha)]$ on the training set, and was all above

0.98 on the test set. The prediction of extrapolated datasets had high R², which showed good performance in estimating the kinetic parameters. This ANN model can be used to predict kinetic parameters of pyrolysis without the traditional method of actual experiments. The kinetic parameters can be obtained from our ANN model with the given data of heat flow, temperature, and corresponding degree of conversion. The performance of our ANN model was good when heating rate was less than 5 °C/min. This is because that the kinetic parameters were very sensitive to the heating rates and highly depending on the heat flow when heating rate was lower than 5 °C/min. However, the kinetic parameters were slightly depending on the heat flow under a higher heating rate, and the performance of ANN model was affected. The model can be coupled with various numerical simulation models to calculate the kinetic parameters with high computational efficiency and accuracy. For example, this ANN model can be incorporated into the pore-scale model describing the thermal decomposition of shale. The investigation of data-driven model can help thoroughly develop the micro pore-scale models for the kerogen pyrolysis modeling. In pore-scale model, the kerogen phase and other impure minerals are separately distributed in the computational domain. The different component of the shale has different reaction kinetics. Thus, it is significant to investigate the reaction kinetics both for the pure kerogen and the shale bulk rock. Within the discretized control volume, the degrees of conversion and temperature vary, because each discretized element has different distance to the heat source. Thus, the trained model can produce the accurate kinetic parameters for each discretized element without conducting multiple experiments.

4. Conclusions

This work investigated the evolution of generated hydrocarbon during the kerogen maturity and established the thermal decomposition kinetics of Green River Shale (Type I kerogen) of the Utah basin. Since the Green River Shale has a high volume of organic matter, which has a high potential to be exploited, we firstly applied the data–driven model to predict the reaction kinetics from the heat flow data of the Green River Shale during the pyrolysis. The obtained results can be incorporated into full physics models to simulate the decomposition of oil shale with high accuracy and faster calculation speed. We investigated the reaction kinetics both for the bulk shale rock and isolated pure kerogen, which can be used in the reservoir–scale models and the pore–scale models. The prediction of extrapolated datasets has excellent performance.

We have the following interesting findings from the investigation. For the pyrolysis of isolated kerogen, we could observe the two–step evolution of hydrocarbons within 200–620 °C of temperature at the heating rate from 5 °C/min to 30 °C/min. However, this two–step mechanism was not apparent for the heating rate higher than 30 °C/min. Under the lower heating rate, the sample had larger weight loss at the end of pyrolysis.

We detected the chemical bonds of C-H, C \equiv N, C=C=N, N3, and C=O from FTIR, which confirmed that the Green River Shale contained alkane, alkene, and aromatics. We also found that Si-O-Si of the Si-O-Si-6 member ring functional groups was strong enough and didn't crack after the pyrolysis. The gas components were analyzed during the pyrolysis at the peaks of derivative of α . We could obtain lots of components at the maximum derivative point. Under the higher heating rate, the more alkane components at the maximum derivative point we can obtain. This was because, the hydrocarbons were generated one by one following their mass weights, and the lighter components were firstly separated before the maximum derivative under the lower heating rates (smaller than 20 °C/min). For the higher heating rates (larger than 20 °C/min), the second-step reaction showed a shorter time, and there was no clear boundary for the generation of different components. C14 was generated continuously during the second-step evolution, which indicated that the Green River Shale contained a plentiful amount of it.

By implementing Friedman method, isoconversional plots and kinetic parameters (activation energy and pre-exponential factors) were obtained from the experimental results. The most probable kinetic models could be selected with higher R² value by using Popescu method. The kinetic parameters obtained from heating the bulk rock were valid for the mixture of organic matter and minerals, while the ones from heating the kerogen samples were valid for the pure organic matter. After obtained the thermal kinetic parameters, we took heat flow rate, $\Delta \alpha$, and heating rate as the input data, and the kinetic parameters as the output data, respectively. The ANN method was used to train the datasets and predict the kinetic parameters. The performance of the data--driven model was good when we randomly selected 20% data as test set to compare the predicted value with the observed data. The R² value could reach 0.99 for training set, and above 0.95 for test set. To see the performance of prediction out of our training set, we picked the data under one designated heating rate as the test set and the remaining data sets as the training set, instead of a random manner. The prediction of extrapolated datasets had high R² when the heating rate was smaller than 5 °C/min, which showed good performance in estimating the kinetic parameters. Then, the degree of conversion of shale with different temperatures and unmeasured heating rates can be predicted by the ANN model. The generated data-driven proxy models can be coupled with full physics models with various scales to simulate the decomposition of oil shale with high accuracy. As such, the kinetic parameters for shale bulk rock and the isolated kerogen can be incorporated into reservoir-scale models and the pore-scale models, respectively.

CRediT authorship contribution statement

Jiahui You: Writing – review & editing, Visualization. **Kyung Jae Lee:** Funding acquisition, Resources, Project administration.

Declaration of Competing Interest

The authors declare that they have no known competing financial interests or personal relationships that could have appeared to influence the work reported in this paper.

Acknowledgements

We greatly appreciate the financial support for this research from National Science Foundation, United States, under Award 2042504 (CAREER: Identifying a New Source of Lithium for Sustainable and Renewable Energy Storage).

Appendix A. Supplementary data

Supplementary data to this article can be found online at https://doi.org/10.1016/j.fuel.2022.123899.

References

- Lee K, Moridis GJ, Ehlig-Economides CA. A Comprehensive Simulation Model of Kerogen Pyrolysis for the In-situ Upgrading of Oil Shales. SPE-134583-PA 2016;21 (05):1612–30.
- [2] Behar F, Vandenbroucke M, Tang Y, Marquis F, Espitalie J. Thermal cracking of kerogen in open and closed systems: determination of kinetic parameters and stoichiometric coefficients for oil and gas generation. Org Geochem 1997;26(5): 321–39.
- [3] Spigolon ALD, Lewan MD, de Barros Penteado HL, Coutinho LFC, Mendonça Filho JG. Evaluation of the petroleum composition and quality with increasing thermal maturity as simulated by hydrous pyrolysis: A case study using a Brazilian source rock with Type I kerogen. Org Geochem 2015;83–84:27–53.
- [4] Zhang T, Wang Z, Wang Y, Wei Z, Li X, Hou X, et al. The characteristics of free/bound biomarkers released from source rock shown by stepwise Py-GC-MS and thermogravimetric analysis (TGA/DTG). J Petrol Sci Eng 2019;179:526–38.
- [5] Kuang W, Lu M, Yeboah I, Qian G, Duan X, Yang J, et al. A comprehensive kinetics study on non-isothermal pyrolysis of kerogen from Green River oil shale. Chemical Engineering Journal 2019;377:120275.

- [6] Tiwari P, Deo M. Compositional and kinetic analysis of oil shale pyrolysis using TGA–MS. Fuel 2012;94:333–41.
- [7] Yan J, Jiang X, Han X, Liu J. A TG-FTIR investigation to the catalytic effect of mineral matrix in oil shale on the pyrolysis and combustion of kerogen. Fuel 2013; 104:307-17
- [8] Pan L, Dai F, Li G, Liu S. A TGA/DTA-MS investigation to the influence of process conditions on the pyrolysis of Jimsar oil shale. Energy 2015;86:749–57.
- [9] Lee KJ. Characterization of Type and Maturity of Organic Matter in Source Rock by In-situ Electrical Heating and Temperature Transient Analysis. SPE International Conference on Oilfield Chemistry. 2019:D011S05R05.
- [10] Sajjad Ahmad M, Liu H, Alhumade H, Hussain Tahir M, Çakman G, Yıldız A, et al. A modified DAEM: To study the bioenergy potential of invasive Staghorn Sumac through pyrolysis, ANN, TGA, kinetic modeling, FTIR and GC–MS analysis. Energy Conversion and Management 2020;221:113173.
- [11] Hosen MA, Hussain MA, Mjalli FS. Hybrid modelling and kinetic estimation for polystyrene batch reactor using Artificial Neutral Network (ANN) approach. Asia-Pac J Chem Eng 2011;6(2):274–87.
- [12] Survey UG. Cumulative oil production reported for Duchesne and Uintah counties; 2014.
- [13] Agency of Petroleum NGaBA. Oil, Natural gas and Biofuels Statistical Yearbook. 2014.
- [14] Ibrahimov RA, Bissada KK. Comparative analysis and geological significance of kerogen isolated using open-system (palynological) versus chemically and volumetrically conservative closed-system methods. Org Geochem 2010;41(8): 800.11
- [15] ASTM. ASTM D6729-14. RESTEK: https://www.restek.com/en/pages/ chromatogram-view/GC_PC1323.
- [16] ASTM. ASTM D2887. https://www.restek.com/en/pages/chromatogram-view/ GC PC1299: RESTEK.
- [17] Claypool GE, Kaplan IR. The Origin and Distribution of Methane in Marine Sediments. In: Kaplan IR, editor. Natural Gases in Marine Sediments. Boston, MA: Springer, US; 1974. p. 99–139.

- [18] Baudin F, Disnar J-R, Aboussou A, Savignac F. Guidelines for Rock-Eval analysis of recent marine sediments. Org Geochem 2015;86:71–80.
- [19] Venkatesh M, Ravi P, Tewari SP. Isoconversional Kinetic Analysis of Decomposition of Nitroimidazoles: Friedman method vs Flynn–Wall–Ozawa Method. J Phys Chem A 2013;117(40):10162–9.
- [20] Bhadeshia HKDH. Neural Networks in Materials Science. ISIJ Int 1999;39(10): 966–79.
- [21] Haykin S. Neural Networks and Learning Machines. New York: 3 Prentice Hall; 2008.
- [22] He K, Zhang Xiangyu, Ren Shaoqing, Sun Jian. Delving Deep into Rectifiers: Surpassing Human-Level Performance on ImageNet Classification. Proceedings of the IEEE International Conference on Computer Vision (ICCV). 2015.
- [23] Kingma DP, Ba J. Adam: A method for stochastic optimization. arXiv preprint arXiv:14126980 2014.
- [24] TensorFlow. TensorFlow.org.; 2015. [Accessed November 10 2015].
- [25] Williams PT, Ahmad N. Investigation of oil-shale pyrolysis processing conditions using thermogravimetric analysis. Appl Energy 2000;66(2):113–33.
- [26] Palayangoda SS, Nguyen QP. THERMAL BEHAVIOR OF RAW OIL SHALE AND ITS COMPONENTS. Oil shale 2015;32(2):160.
- [27] Williams PF. Thermogravimetry and decomposition kinetics of British Kimmeridge Clay oil shale. Fuel 1985;64(4):540–5.
- [28] Haddadin RA, Mizyed FA. Thermogravimetric analysis kinetics of Jordan shale. Ind Eng Chem Process Des Dev 1974;13(4):332–6.
- [29] Doğan ÖM, Uysal BZ. Non-isothermal pyrolysis kinetics of three Turkish oil shales. Fuel 1996;75(12):1424–8.
- [30] Soluions WS. KnowItAll Spectroscopy. https://sciencesolutions.wiley.com/ knowitall-spectroscopy-software/.
- [31] Charlesworth JM. Interaction of clay minerals with organic nitrogen compounds released by kerogen pyrolysis. Geochim Cosmochim Acta 1986;50(7):1431–5.